



## Biomass-derived mesoporous Hf-containing hybrid for efficient Meerwein-Ponndorf-Verley reduction at low temperatures

Hu Li<sup>a,b</sup>, Tingting Yang<sup>b</sup>, Zhen Fang<sup>a,\*</sup><sup>1</sup>

<sup>a</sup> Biomass Group, College of Engineering, Nanjing Agricultural University, 40 Dianjiangtai Road, Nanjing, Jiangsu 210031, China

<sup>b</sup> State-Local Joint Engineering Laboratory for Comprehensive Utilization of Biomass, Center for R&D of Fine Chemicals, Guizhou University, Guiyang 550025, China



### ARTICLE INFO

#### Keywords:

Heterogeneous catalysis  
Biofuels  
Biomass-derived materials  
Self-assembly  
Acid-base bifunctionality

### ABSTRACT

The use of organic chemicals derived from renewable sources to synthesize functional solid materials for heterogeneous catalysis is of great significance. Herein, a new porous and acid-base bifunctional hybrid (FDCA-Hf) was designed and prepared by simple assembly of biomass-derived 2,5-furandicarboxylic acid (FDCA) with hafnium (Hf) under template-free conditions. The resulting FDCA-Hf hybrid with mesopores centered at 6.9 nm, moderate surface area ( $365.8 \text{ m}^2/\text{g}$ ) and acid-base couple sites (density: 0.51 vs 0.97 mmol/g, acid/base molar ratio: 0.53), could selectively catalyze the Meerwein-Ponndorf-Verley reduction of carbonyl compounds under mild reaction conditions (as low as 90 °C in a short time of 1 h), especially of ethyl levulinate to  $\gamma$ -valerolactone, in quantitative yields (95–100%) and relatively higher reaction rate (e.g., turnover frequency:  $2.28 \text{ h}^{-1}$ ) compared to other catalysts. Moreover, the efficient simultaneous (trans)esterification of *Jatropha* oils with high acidic values to biodiesel (up to 98% yield) could also be achieved over FDCA-Hf with robust acid-base catalytic sites. The FDCA-Hf hybrid was highly stable due to the presence of robust metal-organic framework and could be resued with no decline in activity. Further studies demonstrated that the synergistic role of Lewis acid-base couple species ( $\text{Hf}^{4+}-\text{O}^{2-}$ ) and Brønsted acidic species ( $-\text{OH}$ ) of FDCA-Hf contributed greatly to its pronounced catalytic activity.

### 1. Introduction

The exploration of porous carbonaceous materials derived from sustainable lignocellulosic biomass via tandem calcination or pyrolysis and grafting with variable functional species is one of crucial areas in material chemistry, which has been demonstrated to exhibit promising applications in fuel cell, gas adsorption/separation, drug delivery, and catalysis [1–4]. As a more convenient and controllable alternative, the assembly of organic natural molecules such as polyphenol, porphyrin and phytic acid with metal ions (e.g.,  $\text{Cu}^{2+}$ ,  $\text{Fe}^{3+}$ , and  $\text{Zr}^{4+}$ ) is able to mimic natural structures and generate a series of active frameworks with good stability [5–7]. In particular, the diversity of the natural building blocks supplies a broad range of possibilities for the preparation of efficient catalytic materials by coordination with different metal species.

Acid and base dual sites are generally opposing, while the appeared ‘chemical hostility’ can be adjusted into ‘chemical friendliness’ by spatial isolation with a solid support, yolk- or core-shell distribution, and regular lattice arrangement [8–11]. Acid-base bifunctionality is a concept of cooperativity, which typically functions in the models of

dual, sequential or self activation and multi-point stabilization of transition state between two substrates [12]. Via acid-base cooperative catalysis, a variety of reactions can be achieved in high efficiency [13,14]. Amongst them, the Meerwein-Ponndorf-Verley (MPV) and (trans)esterification reactions catalyzed by metal oxides (e.g.,  $\text{ZrO}_2$ ,  $\text{Zr}(\text{OH})_4$  and  $\text{CaLaO}_x$ ) bearing acid-base couple sites have been reported to be chemoselective for the reduction of carbonyl compounds and for biodiesel production, respectively [15–17]. However, the metal oxides in bulky structure normally restrain the sufficient access of acidic and basic centers to the substrates. Harsh reaction conditions, as a remedy, are highly required to give acceptable catalytic performance, but resulting in the easy deactivation of the metal oxides [6]. Therefore, the development of stable and efficient solid acid-base bifunctional catalysts is greatly desirable.

2,5-Furandicarboxylic acid (FDCA) is listed by the U.S. Department of Energy as one of the top-12 valuable molecules from lignocellulose, which is highly stable and can be used in organic synthesis and pharmacology, especially for producing polymers in the replacement of petroleum-based terephthalic acid [18]. Due to the presence of two  $-\text{COOH}$  groups, FDCA is most likely to have the capability in

\* Corresponding author.

E-mail address: [zhenfang@njau.edu.cn](mailto:zhenfang@njau.edu.cn) (Z. Fang).

<sup>1</sup> Web: <http://biomass-group.njau.edu.cn/>.

coordination with metal ions to form organic-inorganic hybrids. This kind of hybrid materials typically possess flexible structure, controllable active species, enhanced catalytic activity, and good thermal and chemical stability, which are typically prepared by using terephthalic acid as organic ligand [19–22]. Herein, a new heterogeneous and porous hafnium 2,5-furandicarboxylate material, denoted as FDCA-Hf, was prepared by simple assembly of  $\text{HfCl}_4$  with FDCA. The high performance of FDCA-Hf in acid-base catalysis was further examined under benign reaction conditions.

## 2. Materials and methods

### 2.1. Materials

Ethyl levulinate (EL, 99%),  $\gamma$ -valerolactone (GVL, 98%), propanal ( $> 99\%$ ), *n*-butanal ( $> 99.5\%$ ), benzaldehyde ( $\geq 99.5\%$ ), *p*-anisaldehyde ( $> 99\%$ ), furfural (FUR,  $\geq 99.5\%$ ), 5-methylfurfural (MF, 98%), 5-hydroxymethylfurfural (HMF,  $> 99\%$ ), naphthalene ( $\geq 99.7\%$ ), citral (97%), cinnamaldehyde ( $\geq 99.5\%$ ), acetophenone ( $\geq 99.0\%$ ), cyclopentanone ( $\geq 99.5\%$ ), dimethyl formamide (DMF, 99.8%), aluminium trichloride ( $\text{AlCl}_3$ , 99%), ferric trichloride ( $\text{FeCl}_3$ ,  $\geq 99.9\%$ ), chromium trichloride ( $\text{CrCl}_3$ , 98%), copper chloride ( $\text{CuCl}_2$ , 98%), zirconium chloride ( $\text{ZrCl}_4$ ,  $\geq 99.9\%$ ), hafnium oxide ( $\text{HfO}_2$ , 99.9%),  $\text{NaHCO}_3$  ( $\geq 99.8\%$ ) and 2-propanol (2-PrOH, 99.5%) were purchased from Shanghai Aladdin Industrial Inc. Terephthalic acid (99%), 2,5-furandicarboxylic acid (FDCA, 97%), formic acid (98%), methanol-d<sub>4</sub> ( $\text{CD}_3\text{OD}$ ,  $> 99.8\%$ ), hafnium tetrachloride ( $\text{HfCl}_4$ ,  $> 99.9\%$ ), 2-propanol-d<sub>8</sub> (2-PrOH-d<sub>8</sub>, 99.5 atom% D), normal methanol (99.9%) and ethanol (AR grade) were bought from Beijing J&K Scientific Ltd. All other chemical reagents were obtained in analytical grade and used as it is, unless otherwise mentioned.

### 2.2. Preparation of different FDCA-M hybrids

All FDCA-M hybrids (M = Hf, Al, Fe, Cr, Cu, Zr) were prepared by the simple assembly of FDCA with an equivalent mole of metal chloride (i.e.,  $\text{HfCl}_4$ ,  $\text{AlCl}_3$ ,  $\text{FeCl}_3$ ,  $\text{CrCl}_3$ ,  $\text{CuCl}_2$  or  $\text{ZrCl}_4$ ) and 0–2.0 mL of formic acid in DMF under solvothermal conditions. In a typical procedure for FDCA-Hf preparation, 1.5 mmol FDCA (0.23 g), 1.5 mmol  $\text{HfCl}_4$  (0.48 g) and 26.5 mmol formic acid (1.0 mL) were dissolved in 15.5 mL DMF (200 mmol) under ambient conditions in a teflon-lined (25 mL) stainless steel autoclave. After vigorously stirring (800 rpm) for 15 min with a magnetic stirrer (IKA, Germany), the tightly sealed autoclave was transferred into a muffle furnace (JZ-4-1200, Shanghai Jingzhao machinery equipment Co. Ltd.) and statically kept for 24 h at 120 °C. Upon completion, the autoclave was taken out and naturally cooled to room temperature, while the resulting white precipitates were filtered (filter paper: 0.22  $\mu\text{m}$ ), successively washed with DMF and ethanol for 3 times, and dried under vacuum conditions at 90 °C for 8 h. For comparison, a conventional  $\text{UiO-66}(\text{Zr})$  organic-inorganic hybrid was prepared by solvothermal treatment of  $\text{ZrCl}_4$  and equimolecular terephthalic acid in DMF at 120 °C under static conditions for 24 h, according to a previously reported synthetic procedure [23]. All the solid samples were dried at 90 °C for 5 h prior to catalyst characterization and analysis of catalytic performance.

### 2.3. Catalyst characterization

The Hf elemental composition was measured by ICP-OES (inductively coupled plasma-optical emission spectrometer) on a Perkin Elmer Optima 5300 DV instrument. FT-IR (Fourier transform infrared spectrometer) spectra were recorded on a Perkin Elmer 1710 spectrometer (KBr disk) in wavenumber range of 400–4000  $\text{cm}^{-1}$ . XRD (X-ray diffraction) patterns of the powder samples were obtained using a Rigaku International D/max-TTR III X-ray powder diffractometer with Cu-K $\alpha$  ( $\lambda = 1.542 \text{\AA}$ ) radiation and  $2\theta$  scanned from 5° to 80°. TEM

(transmission electron microscope) was utilized to study the magnified images using a JEOL JEM-1200EX instrument. FEI Tecnai G2 F30 S-Twin STEM (scanning transmission electron microscope) operating at 300 kV coupled with dispersive X-ray (EDX) was employed to record STEM-HAADF (high-angle annular dark-field) image and elemental mapping. Texture properties including surface areas, pore diameters and pore volumes were tested at –196 °C on a Micromeritics ASAP 2010 sorption analyzer, wherein the volatile impurities in solid samples were removed by heating at 250 °C for 5 h under vacuum before measurement. The thermal property of solid samples was examined by thermogravimetry (TG) analysis on a NETZSCHSTA 429 instrument under N<sub>2</sub> in a flow rate of 30 mL/min at a programmed temperature range of 50–600 °C with a heating ramp of 10 °C/min. XPS (X-ray photoelectron spectroscopy) analysis was conducted on a Physical Electronics Quantum 2000 Scanning ESCA Microprobe (Al-K $\alpha$  anode,  $h\nu = 1486.6 \text{ eV}$ ), and C1s orbital (284.8 eV) was used to correct the binding energy. Surface basicity and acidity of the samples were determined by CO<sub>2</sub>– and NH<sub>3</sub>-TPD (temperature programmed desorption) using a Micromeritics AutoChem 2920 chemisorption analyzer. Regarding the determination details, 10 vol.% CO<sub>2</sub> or NH<sub>3</sub> in Ar with a flow rate of 50 mL/min was adsorbed onto the solid samples at 50 °C for 60 min, followed by purging with Ar (50 mL/min) at 50 °C for another 60 min to remove non-chemically adsorbed CO<sub>2</sub> or NH<sub>3</sub>. TCD signals were recorded by performing CO<sub>2</sub> or NH<sub>3</sub> desorption at a programmed temperature range of 50–300 °C with a heating ramp of 10 °C/min and then kept at 300 °C for 60 min under Ar (flowing rate of 30 mL/min). Molar ratios of Lewis and Brønsted acid sites of the solid Hf-containing samples were measured by pyridine adsorption FT-IR fitted with a Bruker VERTEX V70v system, based on the characteristic peak position and integral area in the wavenumber range of 1400–1700  $\text{cm}^{-1}$ . In a quartz-lined stainless steel IR cell, a similar measurement process of pyridine adsorption at room temperature followed by desorption at 250 °C was adopted.

### 2.4. MPV reduction reactions

The MPV reduction of various aldehydes and ketones using 2-PrOH as hydrogen-donor was carried out in a 25 mL Teflon-lined stainless steel autoclave (WCGF-25, Xi'an Changyi Instrumental Co. Ltd.). In a general reaction procedure, 1.0 mmol EL or other carbonyl compounds, 72 mg solid catalyst, and 5 mL 2-PrOH were added into the autoclave and tightly sealed, followed by heating to a designated temperature of 120–180 °C in 4–9 min. After magnetically stirring at 500 rpm for a reaction time of 0.5–10 h, the autoclave was cooled down to room temperature with tap-water, and the resulting reaction mixtures were quantitatively analyzed by GC (gas chromatography).

### 2.5. Biodiesel production

*Jatropha curcas* L. seed oils with different acid values of 2.5–21.9 mg KOH/g were chosen for the production of biodiesel via simultaneous (*trans*)-esterification. In a general reaction procedure, 2 g *Jatropha* oil with methanol (30:1 methanol/oil molar ratio) and 8 wt% FDCA-Hf were added into the 25 mL Teflon-lined steel autoclave. The resulting mixture placed and sealed in the autoclave was heated to 180 °C within 9 min under vigorously stirring condition (600 rpm). After reacting for 5 h, the autoclave was rapidly cooled down to room temperature by flushing with tap-water before the solid catalyst was separated and recovered from the mixed solution by centrifugation (8000 rpm). The residual liquid mixture was extracted with 5 mL petroleum ether for two times using a separatory funnel to give purified biodiesel (i.e., fatty acid methyl esters; FAMEs) upon using a rotary evaporator connected with a vacuum pump (maximum differential pressure: 98 kPa) for analysis.

## 2.6. Analysis of products

The yields of FAMEs were quantified by  $^1\text{H}$  NMR (nuclear magnetic resonance; deuterated solvent:  $\text{CDCl}_3$ ) on a JEOL NMR spectrometer (500 MHz) by referring to the integral peak areas of  $-\text{OCH}_3$  at 3.65 ppm and  $-\text{CH}_2\text{C}(\text{O})\text{O}-$  at 2.25 ppm, as shown in Fig. S1 with detailed descriptions. For the studied reactions of MPV reduction, liquid substrates, target products and dominant by-products were identified by Agilent 6890N GC–MS (mass spectrometer, 5973 MS). EL, GVL, and other liquid products yielded from different substrates were quantitatively analyzed by Agilent 7890B GC fitted with FID (flame ionization detector) and HP-5 column ( $30\text{ m} \times 0.320\text{ mm} \times 0.25\text{ }\mu\text{m}$ ). The conversions of substrates (e.g., EL) and yields of products (e.g., GVL) were calculated based on standard curves ( $R^2 \geq 0.997$ ) of corresponding commercial samples in five different concentrations along with a certain amount of internal standard (naphthalene).

$$\text{Substrate conversion} = 1 - [(\text{mole of substrate after reaction}) / (\text{mole of initial substrate})] \times 100\% \quad (1)$$

$$\text{Product yield} = (\text{mole of product in the reaction mixture}) / (\text{mole of initial substrate}) \times 100\% \quad (2)$$

$$\text{Product selectivity} = (\text{Product yield}) / (\text{Substrate conversion}) \times 100\% \quad (3)$$

With respect to investigating the reaction pathway for the synthesis of GVL from EL, *ex situ*  $^1\text{H}$  NMR spectra of the reaction mixture volumetrically diluted with  $\text{CD}_3\text{OD}$  after reacting for designated periods ranging from 0.5 to 4 h were performed to observe characteristic peaks of protons in different groups, based on the specific chemical shift values. In addition,  $^1\text{H}$  NMR spectra were also recorded for the reaction mixture performed in  $2\text{-PrOH-}d_8$  after 0.5–4 h to study isotopic kinetics of EL-to-GVL conversion. To elucidate the proceeding of direct hydrogen transfer process, mass analysis of GVL formed from catalytic transfer hydrogenation of EL in isotopic  $2\text{-PrOH-}d_8$  was further conducted with GC–MS.

## 2.7. Catalyst recycles

After each cycle of catalytic reactions, the solid catalyst dispersed in the reaction mixture was separated and recovered by centrifugation (8000 rpm) for 5 min, successively washing with ethanol and acetone for 3 times, and finally drying under vacuum at 80 °C for 5 h. The resulting solid sample was directly employed for the next run of reaction. Prior to ICP analysis of Hf species leached into the reaction solution, the filtrate was volumetrically diluted with water after removal of solid residue by filtration.

## 3. Results and discussion

### 3.1. Catalyst characterization

#### 3.1.1. Textural and structural properties

The prepared FDCA-Hf was initially characterized by SEM, TEM, STEM-HAADF,  $\text{N}_2$  adsorption-desorption, FT-IR, and XRD techniques, and the results are shown in Fig. 1. The FDCA-Hf hybrid was formed in porous surface (Fig. 1A), small particles with a diameter of around 10 nm (Fig. 1B), and the even connection of FDCA with Hf species (Fig. 1C). In contrast, the sole  $\text{HfO}_2$  was in bulky structure (Figs. S2–S4). Moreover, FDCA-Hf had a much higher surface area (365.8 vs 23.1  $\text{m}^2/\text{g}$ ) and pore volume (0.63 vs 0.17  $\text{cm}^3/\text{g}$ ), as well as more centered mesopores (6.9 vs 28.9 nm), in comparison with  $\text{HfO}_2$  (Fig. 1D, Table 1). FT-IR spectrum of FDCA-Hf in Fig. 1E reveals the symmetric and asymmetric stretching vibration of the  $-\text{CO}_2-$  group at 1420 and 1500–1700  $\text{cm}^{-1}$ , respectively [24]. Notably, the bridging coordination mode of FDCA to Hf (see schematic in Fig. 1E) could be verified by a

splitting of about 160  $\text{cm}^{-1}$  between the symmetric and asymmetric peaks (Fig. 1E), which is in close agreement with the  $\text{UiO-66}$  structure [25]. In contrast, only single stretching vibrations with a split of 250  $\text{cm}^{-1}$  were observed in the case of FDCA, in close agreement with the monodentate C–OH ( $\nu$ : 2500–3200  $\text{cm}^{-1}$ ) of carboxyl groups in FDCA [25]. Relatively lower intensities for the furan-ring (740–800, 870–885, and 1015–1030  $\text{cm}^{-1}$ ) and C–O bond (1100–1270  $\text{cm}^{-1}$ ) vibrations of FDCA-Hf were observed, clearly demonstrating the tight combination of FDCA with Hf species. On the other hand, FDCA-Hf was found to have obvious redshifts in stretching vibrations of  $-\text{CO}_2-$  groups with relatively higher intensity compared with sole FDCA, further confirming the bridging coordination between Hf and carboxyl groups of FDCA. With respect to  $\text{HfO}_2$ , the absorptions at around 3430 and 1630  $\text{cm}^{-1}$  were assigned to the stretching vibrations of the  $-\text{OH}$  groups and the bending vibration of water molecules, respectively (Fig. 1E). Likewise, a small broad band at  $\sim 3400\text{ cm}^{-1}$  for FDCA-Hf might contribute to the protonated carboxyl groups ( $-\text{CO}_2\text{H}$ ) of FDCA moieties which are incompletely coordinated with Hf [25]. It is worth noting that the blueshift in the stretching vibrations of hydroxy groups for FDCA-Hf relative to that of pure FDCA implies the presence of unstable  $-\text{OH}$  species, possibly corresponding to weak Brønsted acidic sites. In addition, the hybrid was amorphous (Fig. 1F), further affirming the presence of defects or irregular connectivity, which is unlike  $\text{HfO}_2$  having high crystallinity (Fig. 1F) with clear crystal lattice (Fig. S5).

#### 3.1.2. Stability and acid-base properties

The thermal stability of FDCA-Hf and  $\text{HfO}_2$  was examined by TG analysis in the range of 50–600 °C. Fig. 2A shows that the decomposition temperature of FDCA-Hf reaches to 328 °C, which can be ascribed to the lattice change at 328–350 °C and the degradation of organic-matter at 350–450 °C. It should be noted that the weight of FDCA-Hf decreased by about 10% in the temperature range of 50–328 °C, which is a little higher than  $\text{HfO}_2$  (ca. 7% weight loss). This is possibly due to the removal of extra weak Brønsted acidic species ( $-\text{OH}$ ) and organic residues (e.g., DMF) inside pores of FDCA-Hf besides physically adsorbed water, in accordance with the results obtained by FT-IR and  $\text{N}_2$  adsorption-desorption (Fig. 1D and E). As such,  $\text{CO}_2$ - and  $\text{NH}_3$ -TPD were conducted in the desorption temperature range of 50–300 °C and keeping at 300 °C for 60 min to determine the density of base and acid sites, respectively. Table 1 shows that FDCA-Hf possesses relatively higher contents of both acidic (0.51 vs 0.16  $\text{mmol/g}$ ) and basic (0.97 vs 0.24  $\text{mmol/g}$ ) species but slightly lower acid/base molar ratio (0.53 vs 0.67), as compared with  $\text{HfO}_2$ . This could be ascribed to the formation of robust Hf-O-C frameworks that bear more thermally resistant both acidic ( $\text{Hf}^{4+}$ ) and basic ( $\text{O}^{2-}$ ) species during solvothermal treatment of FDCA and  $\text{HfCl}_4$ . To further examine the strength of these formed acid and base sites in FDCA-Hf, XPS was used to evaluate the relative binding energy values of Hf 4f (Fig. 2B) and O 1s (Fig. 2C). In comparison with  $\text{HfO}_2$ , the Hf species in FDCA-Hf was found to have a larger positive charge based on higher Hf 4f binding energies (Fig. 2B), clearly indicating the relatively stronger Lewis acidity [26]. On the other hand, a lower basicity of oxygen species in Hf-O-C framework of FDCA-Hf was observed on the basis of a relatively higher O 1s binding energy than  $\text{HfO}_2$  (532.2 eV vs 530.5 eV), which was corresponding to a lower negative charge (Fig. 2C) [27]. Relatively higher acid strength but lower base strength distributed on solid catalytic materials were speculated to be favorable for the transfer hydrogenation and the suppression of side reactions like condensation especially caused by strong basic species [4,27]. All these parameters demonstrated that FDCA-Hf might be highly active for acid-base cooperative catalysis. For comparison, other FDCA-metal (Al, Cr, Fe, Cu, Zr) hybrids were also prepared with variable acid/base properties (Table S1), manifesting that the coordination ability of carboxylate to metal species directly affected both acidity and basicity of the hybrid.

In addition, the presence of Brønsted acidic sites was also demonstrated to be helpful for the Lewis acid-mediated hydrogen-transfer

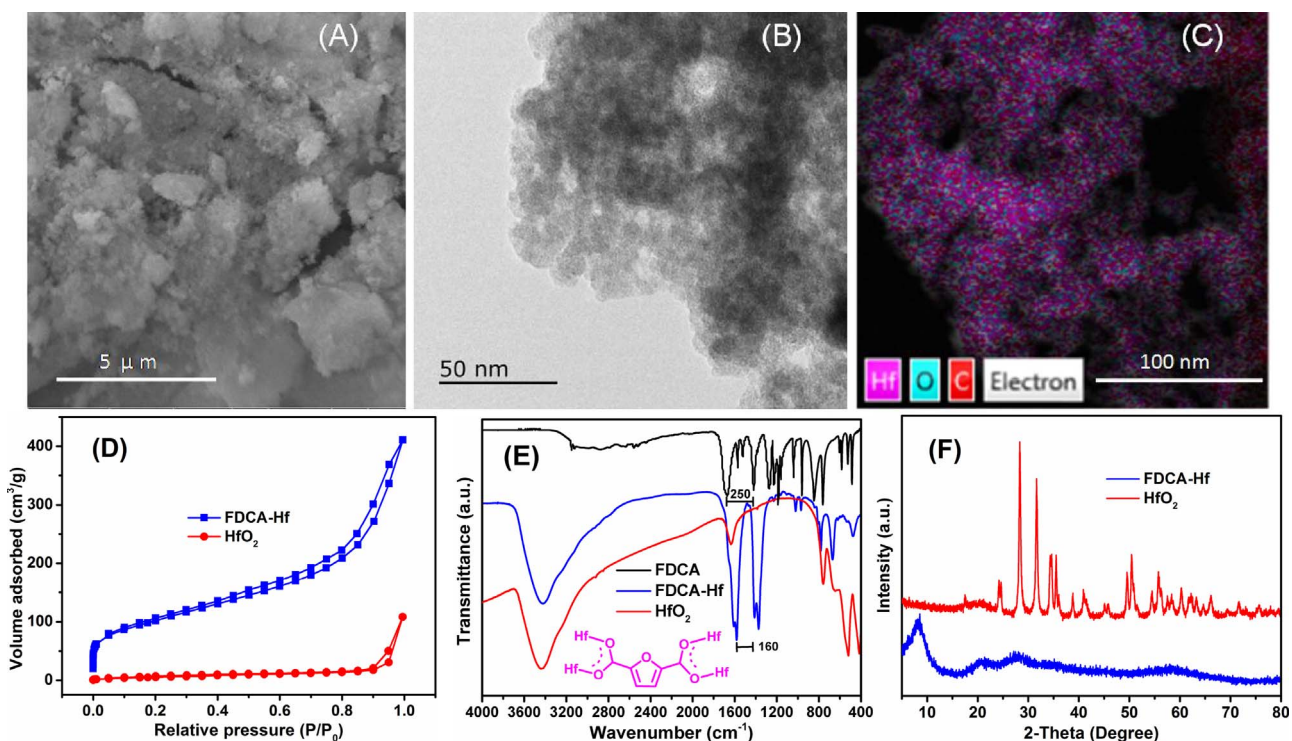


**Fig. 1.** Texture and structural characterization of the prepared FDCA-Hf and  $\text{HfO}_2$ : (A) SEM image, (B) TEM image, (C) STEM -HAADF image with elemental mapping, (D)  $\text{N}_2$  adsorption-desorption isotherms, (E) FT-IR spectra, and (F) XRD patterns.

**Table 1**  
Surface area, volume and porosity of different catalysts.

Catalyst	$S_{\text{BET}}$ ( $\text{m}^2/\text{g}$ ) <sup>a</sup>	$V_{\text{pore}}$ ( $\text{cm}^3/\text{g}$ ) <sup>b</sup>	$D_{\text{mean}}$ (nm) <sup>c</sup>	Basicity (mmol/g) <sup>d</sup>	Acidity (mmol/g) <sup>d</sup>	Acid/ base ratio
FDCA-Hf	365.8	0.63	6.9	0.97	0.51	0.53
$\text{HfO}_2$	23.1	0.17	28.9	0.24	0.16	0.67
FDCA-Zr	170	0.15	3.5	0.80	0.67	0.84
UiO-66(Zr)	1446	0.61	1.7	0.69	0.77	1.12
FDCA-Hf <sup>e</sup>	343.7	0.61	7.1	0.91	0.49	0.54

<sup>a</sup> BET surface area was obtained from  $\text{N}_2$  adsorption isotherm.

<sup>b</sup> Volume of pores was estimated from BJH Adsorption cumulative volume of pores.

<sup>c</sup> Average pore size was estimated from the adsorption average pore diameter.

<sup>d</sup> Basicity and acidity of the catalysts were determined by  $\text{CO}_2^-$  and  $\text{NH}_3$ -TPD, respectively, with a programmed temperature: heating from 50 to 300 °C at a rate of 10 °C/min and then kept at 300 °C for 60 min gas desorption.

<sup>e</sup> Recovered FDCA-Hf in the sixth cycle.

process [28–30]. Hereby, pyridine-adsorbed FT-IR spectra of both FDCA-Hf and  $\text{HfO}_2$  were recorded at a desorption temperature of 250 °C after pyridine adsorption and completely purging with Ar, as provided in Fig. 2D. As expected, FDCA-Hf was found to have increased acid density of both Lewis and Brønsted acid sites, as compared with  $\text{HfO}_2$ , by referring to the integral areas of bands at wavenumber of 1450 and 1545  $\text{cm}^{-1}$ , respectively (Fig. 2D). It was also worth noting that relatively larger bands at around 1580  $\text{cm}^{-1}$  and 1620  $\text{cm}^{-1}$  of FDCA-Hf than those of  $\text{HfO}_2$ , which were assigned to hydrogen-bonded pyridine and pyridine-adsorbed on Lewis acidic centers, respectively [31], further demonstrated higher Brønsted and Lewis acid strength of the former. As consistent supplements to FT-IR (Fig. 1E) and XPS (Fig. 2B & C) spectra, the results of pyridine-adsorbed FT-IR (Fig. 2D) proved the simultaneous presence of protonated carboxyl groups ( $-\text{CO}_2\text{H}$ ) of FDCA moieties and Hf-O-C frameworks, which contributed to the formation of Brønsted acidic species and Lewis acid/base sites, respectively.

### 3.2. Activity of different catalysts

Catalytic transformation of sugar-derived levulinic acid and its esters into GVL is one of the crucial reactions for biomass valorization, which involves the cascade hydrogenation of acetyl group and lactonization [32,33]. Herein, the conversion of EL to GVL was chosen as the model reaction to study the catalytic performance of FDCA-Hf in the MPV reduction (Table 2) and the influence of different reaction parameters. In Table 2, the absence of catalyst did not give any GVL from EL at 160 °C for 4 h (entry 1). Among the tested catalysts, FDCA-Hf exhibited the best activity with a pronounced GVL yield of 98%, turnover frequency (TOF) of  $2.28 \text{ h}^{-1}$ , and reaction rate constant ( $k$ ) of  $431.6 \times 10^{-6} \text{ s}^{-1}$  (entry 2). In contrast, other metal-FDCA hybrids were not active for the reaction under the identical conditions (entries 3–6). The higher performance of FDCA-Hf catalyst was most likely to be positively correlated with a relatively lower acid/base molar ratio (0.53), while the presence of more acid sites relative to base ones (2.38–11.57) was helpful for the formation of isopropyl levulinate (IPL, 4–6% yields) via the transesterification of EL with 2-PrOH. Although FDCA-Zr, UiO-66(Zr) and  $\text{HfO}_2$  had comparable acid/base ratios (0.67–1.12) to FDCA-Hf, the resulting inferior selectivity and yield of GVL (entries 7–9) could be ascribed to their higher base strength as illustrated by XPS (Fig. S6) that might promote the transesterification to yield more IPL, besides less density of acid/base sites, lower BET surface area or smaller pore size (Table 1).

As discussed vide supra, the protonated carboxyl groups ( $-\text{CO}_2\text{H}$ ) of FDCA moieties in the FDCA-Hf hybrid might result in the formation of Brønsted acidic species, as elucidated by pyridine-adsorbed FT-IR spectra with a desorption temperature of 250 °C in Fig. 2D. On the other hand, the FDCA-Hf dried at 90 °C possibly contained a certain amount of hydroxy groups on the surface of Hf species [34], which might act as weak Brønsted acid to participate in the reaction process. To examine the possible role of both strong and weak Brønsted acid sites for the conversion of EL to GVL, three control experiments were thus carried out. The as-prepared FDCA-Hf hybrid was calcined at 300 °C in  $\text{N}_2$  atmosphere for 5 h to partially remove weak surface hydroxy groups [34],

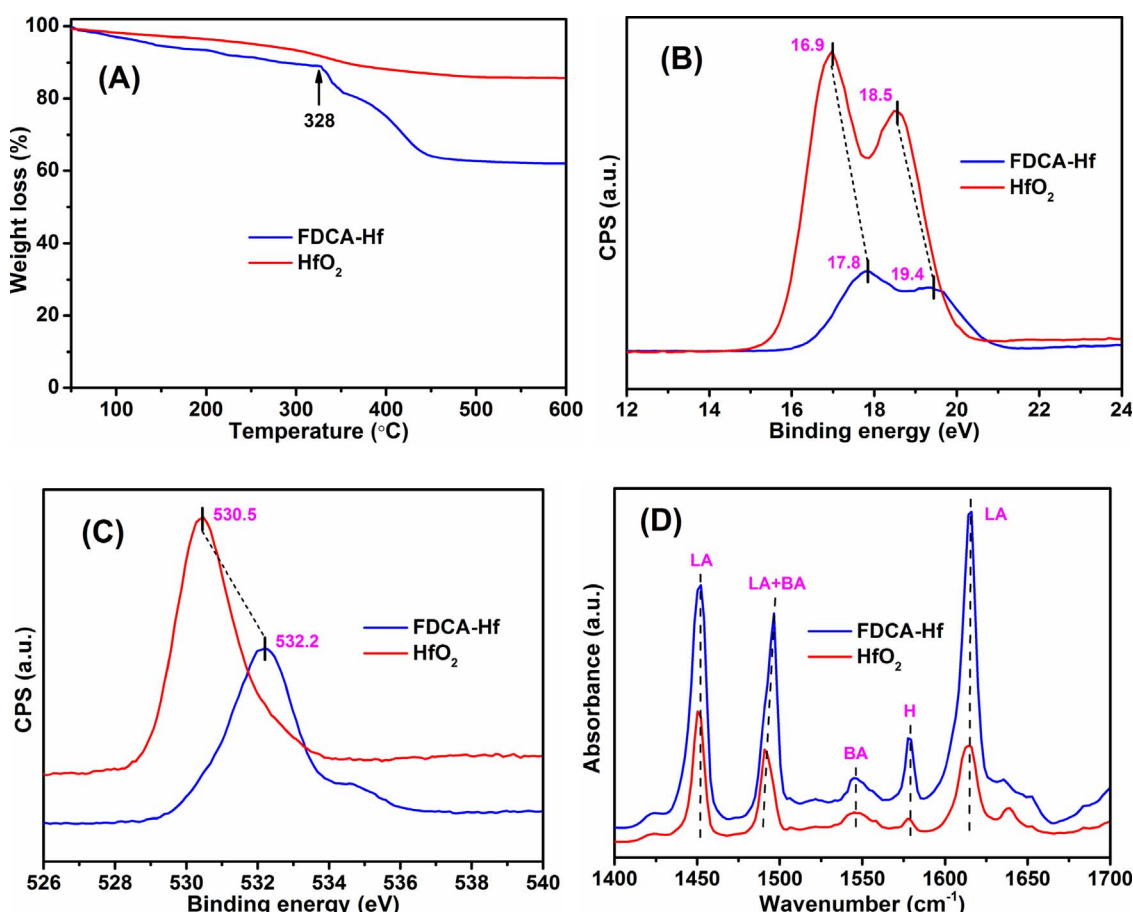


**Fig. 2.** Thermostability and acid-base properties of the prepared FDCA-Hf and HfO<sub>2</sub>: (A) TG curves, (B) XPS spectra of Hf 4f, (C) XPS spectra of O 1s, and (D) Pyridine-adsorbed FT-IR spectra (LA: Lewis acid, BA: Brønsted acid, H: hydrogen-bonded pyridine).

and the resulting catalyst was denoted as FDCA-Hf-300. In order to selectively poison the carboxylic acid groups on the FDCA-Hf hybrid, 100 mg of the hybrid was stirred in 0.05 mol/L NaHCO<sub>3</sub> aqueous solution (50 mL) at room temperature for 24 h, washed with de-ionic water, and dried at 90 °C under vacuum for 8 h to give FDCA-Hf-Na (where R-COOH + NaHCO<sub>3</sub> → RCOONa + CO<sub>2</sub> + H<sub>2</sub>O) [35], followed by calcination at 300 °C in N<sub>2</sub> for 5 h to prepare FDCA-Hf-Na-300 free of both carboxyl and hydroxy groups. Under the above identical reaction conditions (160 °C for 4 h), all three catalysts (FDCA-Hf-Na, FDCA-Hf-300 and FDCA-Hf-Na-300) were observed to have inferior activity to the pristine FDCA-Hf with respect to the yields of GVL obtained from EL, which is in the order of FDCA-Hf-Na-300 (83%) < FDCA-Hf-Na (87%) < FDCA-Hf-300 (95%) < FDCA-Hf (98%). These results

clearly indicated that both weak (minor) and strong (dominant) Brønsted acid species played a positive role in the production of GVL from EL, wherein the promotion effect of carboxyl groups in FDCA-Hf could also lead to the superior catalytic performances to HfO<sub>2</sub> and other tested catalysts. On the other hand, it is also worth noting that the moderate GVL yield of 83% with FDCA-Hf-Na-300 after the removal of both weak and strong Brønsted acid sites from FDCA-Hf can still be obtained, further indicating the principal role of Lewis acid and base sites in the acceleration of GVL formation from EL.

### 3.3. Effect of acid/base site ratio in FDCA-Hf

To further elucidate the effect of acid/base site ratio of FDCA-Hf on

**Table 2**

Catalytic conversion of EL to GVL with different catalysts.<sup>a</sup>

Entry	Catalyst	GVL yield (%)	GVL selec. (%)	EL conv. (%)	TOF (h <sup>-1</sup> ) <sup>b</sup>	10 <sup>-6</sup> × k (s <sup>-1</sup> ) <sup>c</sup>	Acid/base ratio	IPL yield (%)
1	Blank	0	0	< 1	–	0.5	–	–
2	FDCA-Hf	98	98	> 99	2.28	431.6	0.53	1( ± 0.3)
3	FDCA-Al	5	45	11	0.18	8.1	2.38	4( ± 0.6)
4	FDCA-Fe	3	30	10	0.13	7.3	3.58	5( ± 1.4)
5	FDCA-Cr	1	14	7	0.04	5.0	8.22	5( ± 0.7)
6	FDCA-Cu	< 1	8	9	0.03	6.5	11.57	6( ± 1.2)
7	FDCA-Zr	63	86	73	1.49	90.9	0.84	8( ± 2.1)
8	UiO-66(Zr)	52	68	76	1.24	99.1	1.12	19( ± 2.8)
9	HfO <sub>2</sub>	22	79	28	1.91	22.8	0.67	4( ± 1.1)

<sup>a</sup> Reaction conditions: 1 mmol EL, 72 mg catalyst, 5 mL 2-PrOH, 160 °C, and 4 h.

<sup>b</sup> TOF = (mole of GVL)/(mole of acid/base sites × time).

<sup>c</sup> Reaction rate constant k is obtained from –ln (1 – EL conversion) vs time.

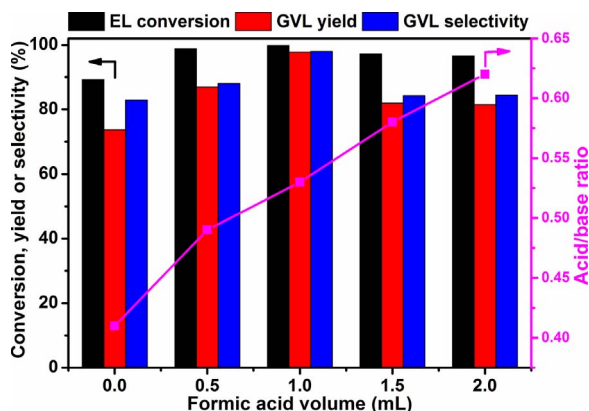


**Fig. 3.** Effect of formic acid dosage used for FDCA-Hf preparation on the conversion of EL to GVL; Reaction conditions: 1 mmol EL, 72 mg FDCA-Hf (16 mol% Hf), 5 mL 2-PrOH, 160 °C, and 4 h.

the EL-to-GVL conversion, the distribution of acid and base species was adjusted by the addition of different volumes of formic acid (0–2.0 mL) into the mixture of precursors for the preparation of FDCA-Hf under otherwise identical solvothermal synthetic conditions (Fig. 3). The ratio of acid/base sites separately determined by NH<sub>3</sub>/CO<sub>2</sub>-TPD was observed to almost linearly increase from 0.41 to 0.62 with the increase of formic acid volume (Table S2), and both GVL yield/selectivity (98%/98%) and EL conversion (100%) reached the highest values at 160 °C in 4 h when 1.0 mL of formic acid was used, corresponding to the acid/base site ratio of 0.53 in FDCA-Hf. Either a low or high acid/base site ratio led to the decreased activity (Fig. 3), further indicating the synergistic role of acid and base sites with an appropriate molar ratio in the conversion of EL to GVL. In order to elucidate the possible reason for the relative increase in acidity to basicity, the acidic type of the FDCA-Hf hybrids prepared using different volumes of formic acid was further examined by pyridine-adsorbed FT-IR. It was found that the molar ratio of Lewis/Brønsted acid sites greatly decreased from 7.9 to 4.3 with the addition of formic acid increasing from 0 to 2.0 mL (Table S2), and the optimal Lewis/Brønsted acid site ratio was 6.8. The co-addition of formic acid seems to compete with carboxyl groups in FDCA to coordinate to metal ions (Hf<sup>4+</sup>), thus resulting in the formation of structural defects and free –COOH species [36–38]. Unfortunately, Brønsted acidic species were most likely to be generated by the consumption of Lewis acid sites, which on the other hand significantly restrained the occurrence of MPV reduction that is initially activated by Lewis acidic catalyst [39]. Therefore, the presence of both base and Brønsted acid sites played promotion effect in the synthesis of GVL from EL, while Lewis acidic species seemed to be dominant factor to activate the MPV reduction. It was worth noting that GVL yield was observed to decrease by 35% and 42% when acid and base sites of FDCA-Hf were poisoned by adding superfluous pyridine and benzoic acid (same mass weight to the catalyst), respectively, according to a previously reported method [40]. This result, in combination with the speculation in Section 3.2, shows that both Lewis acid and base sites are more crucial than Brønsted acidic species in the synthesis of GVL from EL. Considering above discussions, it can be deduced that Lewis acid sites may be responsible for activating MPV reduction of EL in the assistance of base sites, while Brønsted acid sites (or in company with base sites) are able to primarily catalyze the succedent lactonization, further facilitating the migration of reaction equilibrium to GVL since both MPV reduction and lactonization reactions are reversible.

#### 3.4. Effect of reaction temperature and time

The influence of reaction temperature and time on the synthesis of GVL from EL over FDCA-Hf was also examined (Fig. 4). GVL in high yields of 85% and 97% could be obtained under mild conditions (e.g.,

120 and 140 °C for 10 h, respectively). This further indicated the superior activity of the as-prepared FDCA-Hf bearing both acid and base sites in the conversion of EL to GVL in comparison with previously reported results, where ≥150 °C reaction temperatures were involved (Table S3) [6,40–50]. Besides the formation of GVL, IPL was observed to be the dominant byproduct especially at a low temperature of 120 or 140 °C in a short reaction time (1–4 h), which could be formed through lactonization catalyzed by Brønsted acid or Lewis base sites. It was interesting to note that IPL could be further converted to GVL by prolonging the reaction duration and raising the temperature (Fig. 4), showing the robust capability of Lewis acid sites in promoting MPV reduction although the side reaction takes place over Brønsted acid or Lewis base sites at the early stage of low-temperature reaction mixtures. Notably, nearly 100% mass balance was detected for all conducted experiments. These results show that the biomass-derived acid-base bifunctional catalyst FDCA-Hf can be a promising candidate for MPV reduction, transesterification (lactonization), and other relevant reactions, in view of its high sustainability and reactivity.

#### 3.5. Catalyst recycle study

The use of catalyst in a low amount was favorable to reduce the production cost, while it may also restrain the activity of the catalyst. Gratifyingly, 9 mg of FDCA-Hf (2 mol% Hf) could afford GVL in a good yield of 77% with 85% selectivity after reacting at 160 °C for 4 h (Fig. S7). The increase of catalyst dosage from 9 mg to 72 mg (16 mol% Hf) significantly improved the yield of GVL to 98%, and then leveled off by using 144 mg of FDCA-Hf (32 mol% Hf). The catalyst recycle study was thus carried out with the optimal FDCA-Hf dosage of 72 mg (16 mol% Hf) at 160 °C after 4 h. It was shown that FDCA-Hf was able to be reused for at least six times with no noticeable decrease in catalytic performance (Fig. 5), and the concentration of Hf leached into reaction mixture was extremely low (< 0.3 ppm) as detected by inductively coupled plasma-optical emission spectrometer (ICP-OES). Moreover, the recovered FDCA-Hf in the sixth cycle was characterized by FT-IR, XRD, N<sub>2</sub> adsorption-desorption, NH<sub>3</sub>/CO<sub>2</sub>-TPD, and TG analyses (Fig. 6, Table 1), and the results testified that the structural, textural (BET surface area: 365.8 vs 343.7 m<sup>2</sup>/g; pore volume: 0.63 vs 0.61 cm<sup>3</sup>/g; pore size: 6.9 vs 7.1 nm), and acidic/basic properties (acidity: 0.51 vs 0.49 mmol/g; basicity: 0.97 vs 0.91 mmol/g; acid/base ratio: 0.53 vs 0.54) of the fresh and used FDCA-Hf catalysts remained no evident change after six consecutive cycles. Notably, the slight weight loss of recovered FDCA-Hf catalyst relative to that of the fresh counterpart indicated the adsorption of organic species in small amount, which may partially block the access of active sites, thus contributing to the marginal decrease of catalytic activity.

#### 3.6. Reaction mechanism study

To elaborate the reaction pathway, *ex situ* <sup>1</sup>H nuclear magnetic resonance (NMR) spectra for the reaction mixture of EL-to-GVL conversion were monitored at different times of 0.5–4 h and volumetrically diluted by CD<sub>3</sub>OD (Fig. S8). It was observed that GVL was gradually formed by referring to the increase of its characteristic peaks at around 5.2 and 2.1 ppm with the extension of reaction time, despite the bands of EL being overlapped with those of other molecules (Fig. S8). For more clear clarifications, the catalytic conversion of EL to GVL with FDCA-Hf in 0.5–4 h was also performed in 2-PrOH-*d*<sub>8</sub> and recorded by <sup>1</sup>H NMR (Fig. S9). By referring to the NMR spectra of pure 2-PrOH-*d*<sub>8</sub>, and EL, GVL and ethanol in 2-PrOH-*d*<sub>8</sub>, it can be observed that the peaks of protons assigned to –CH<sub>3</sub> (**1a**), –C(=O)–CH<sub>2</sub>– (**4a**) and –O–CH<sub>2</sub>– (**5a**) of EL gradually decrease till disappearance with the possibly increasing addition of deuterium (D) from isotopic 2-PrOH-*d*<sub>8</sub> to form GVL by prolonging the reaction time from 0.5 to 4 h (Fig. S9). As a result, chemical shifts of –CH<sub>3</sub>–C(=O)– (**2a**), –O–C(=O)–CH<sub>2</sub>– (**3a**) and –C(=O)–CH<sub>2</sub>– (**4a**) protons of EL toward –CH<sub>3</sub> (**1b'**),

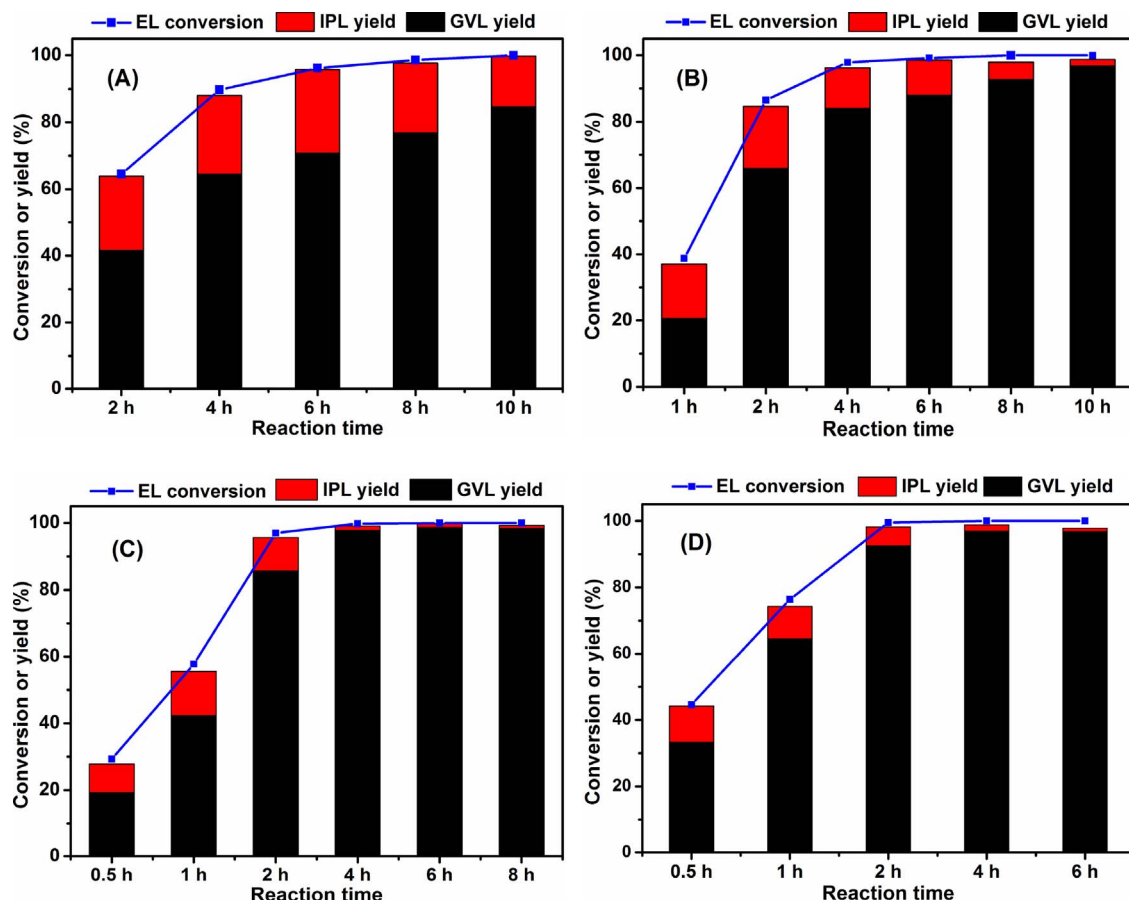


**Fig. 4.** Effect of reaction time on the conversion of EL to GVL at variable temperature: (A) 120 °C, (B) 140 °C, (C) 160 °C, and (D) 180 °C; Reaction conditions: 1 mmol EL, 72 mg catalyst (16 mol% Hf), and 5 mL 2-PrOH.

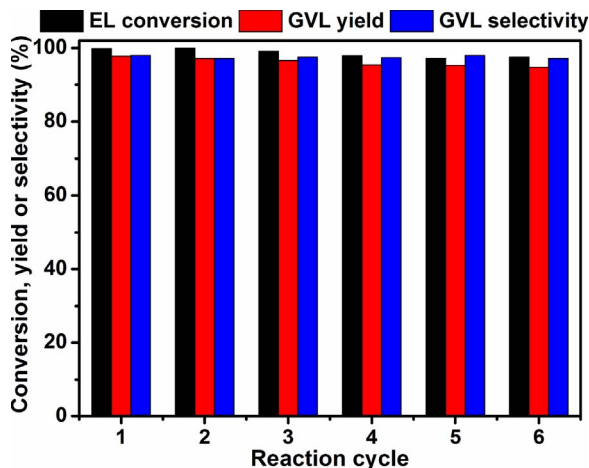


**Fig. 5.** Reusability of FDCA-Hf in the conversion of EL to GVL; Reaction conditions: 1 mmol EL, 72 mg FDCA-Hf (16 mol% Hf), 5 mL 2-PrOH, 160 °C, and 4 h.

$-\text{O}-\text{C}(=\text{O})-\text{CH}_2-$  (**3b'**) and  $-\text{CH}_2-$  (**2b'**) protons of GVL formed from EL using 2-PrOH- $d_8$  as both solvent and H-donor can be observed, respectively. Likewise, slight chemical shifts between GVL formed in 2-PrOH- $d_8$  and normal GVL also occur. That is possibly due to the incorporation of D into GVL, as proved by the absence of **4a'** proton throughout the reaction mixture (Fig. S9), despite of their similar proton environments. Accordingly, MS spectrum shows the presence of an additional 1 amu ( $m/z = 101$ ) for the generated GVL (Fig. S10), explicitly substantiating the proceeding of hydrogen transfer process. In addition, the gradual increase of proton intensity belonging to EtOH at

around 5.7 ppm (Fig. S9) indicates the occurrence of intramolecular transesterification (lactonization).

As discussed *vide supra*, the Lewis/Brønsted acid (originating from  $\text{Hf}^{4+}$  and  $-\text{OH}$ , respectively) and base (originating from  $\text{O}^{2-}$  in carboxyl groups) couple sites are crucial for the cascade transfer hydrogenation and lactonization of EL to GVL. For the possible reaction mechanism, it can be proposed that the adsorption of 2-PrOH onto FDCA-Hf assisted with Lewis acid-base sites ( $\text{Hf}^{4+}-\text{O}^{2-}$ ) leads to the formation of isopropoxide and hydride by dissociation, while the carbonyl group in EL possibly anchored by Brønsted acidic species [51,52] was simultaneously activated by  $\text{Hf}^{4+}$ , thus generating a six-link intermediate to facilitate the hydrogen transfer route (Fig. 7). Then, the resulting 4-hydroxypentanoate is further converted to GVL via intramolecular transesterification promoted by both basic sites and Brønsted acidic species generated from structural defect [53,54]. Although the cascade reaction steps are reversible, the lactonization process is most likely to facilitate the reaction equilibrium being shifted to GVL formation [55–57]. In parallel, IPL derived from EL over acidic or strong basic sites via transesterification [58,59] can also yield GVL through the identical tandem reaction process (Fig. 7).

### 3.7. Substrate scope expansion

Encouraged by the pronounced activity of FDCA-Hf in the MPV reduction and intramolecular transesterification of EL to GVL, the scope of substrates was further extended to other biomass-derived carbonyl compounds (Table 3). It can be observed that aliphatic and aromatic aldehydes can be effectively hydrogenated to corresponding alcohols at 90 or 100 °C in 1 h (entries 1–4). Relatively harsh conditions of 100 °C for 2–5 h were required for achievement of comparable activity in the

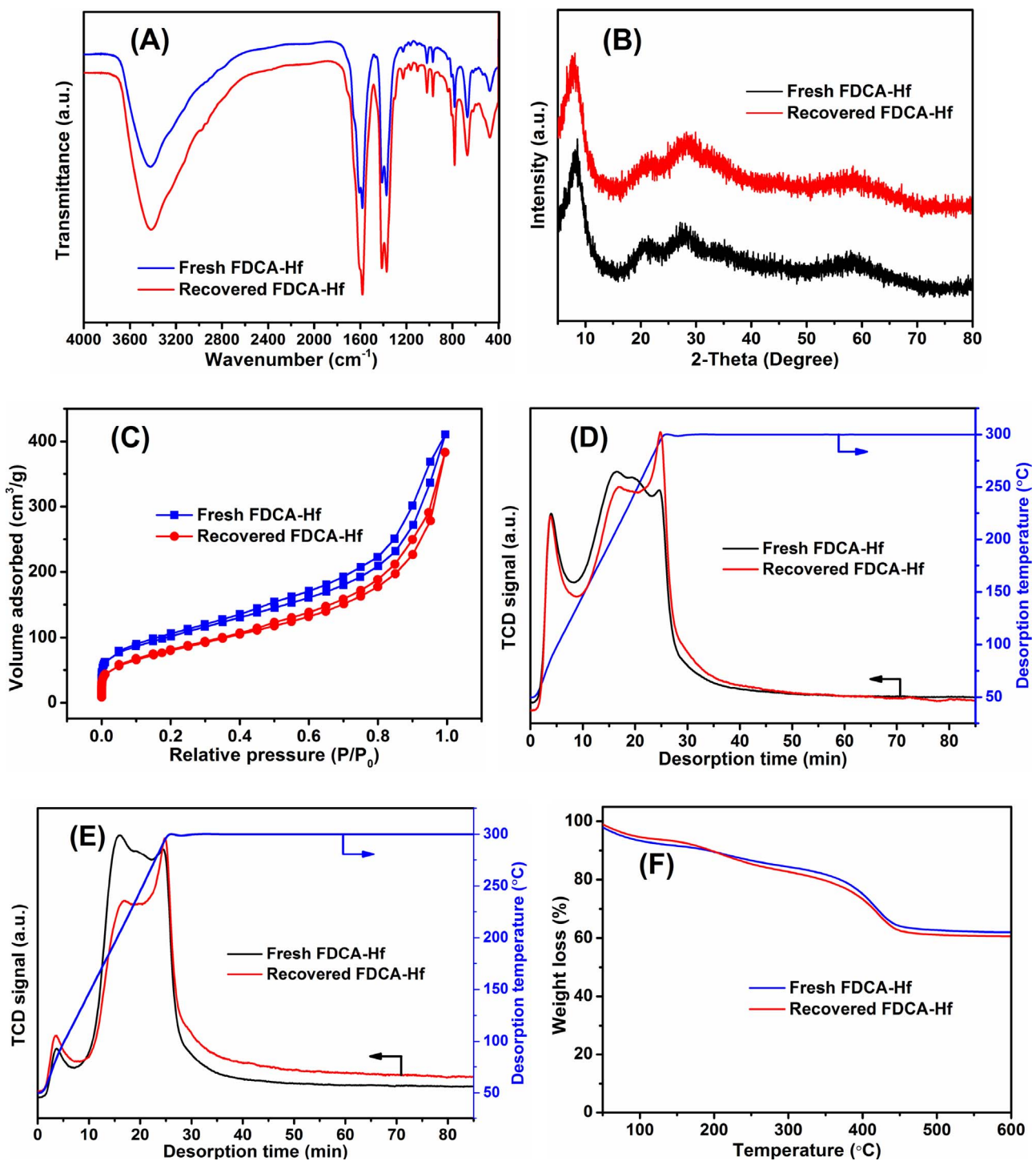


**Fig. 6.** Analyses of fresh and recovered FDCA-Hf hybrids after six cycles: (A) FT-IR spectra, (B) XRD patterns, (C)  $N_2$  adsorption-desorption isotherms, (D)  $NH_3$ -TPD curves, (E)  $CO_2$ -TPD curves, and (F) TG curves.

MPV reduction of furanic aldehydes (entries 5–8). The compounds containing an adjacent double bond (entries 9–10) or ketones (entries 11–12) subjected to MPV reduction also needed a longer reaction time or higher temperature, which was possibly attributed to the occupation of the Lewis acid centers with the double bond or the steric hindrance to lower the probability of carbonyl groups accessible to the active centers, respectively. These results demonstrate the universality of FDCA-Hf in the MPV reduction of carbonyl compounds under mild reaction conditions.

Apart from MPV reduction, the catalytic performance of FDCA-Hf in

the (trans)esterification was also investigated. In Fig. S11, FDCA-Hf could efficiently catalyze simultaneous (trans)esterification of *Jatropha* oil in different acid values (2.5–21.9 mg KOH/g) with methanol to produce biodiesel in yields of 83–98% at 180 °C for 5 h, which possibly implied the sufficient and robust acidity and basicity of the hybrid for the catalytic valorization of acidic oils. In order to make clear whether Lewis acid sites played a role in the (trans)esterification, both weak and strong Brønsted acid species were poisoned by successive treatment with  $NaHCO_3$  and calcination at 300 °C to give FDCA-Hf-Na-300 using the method described in Section 3.2, while the overall acid and base

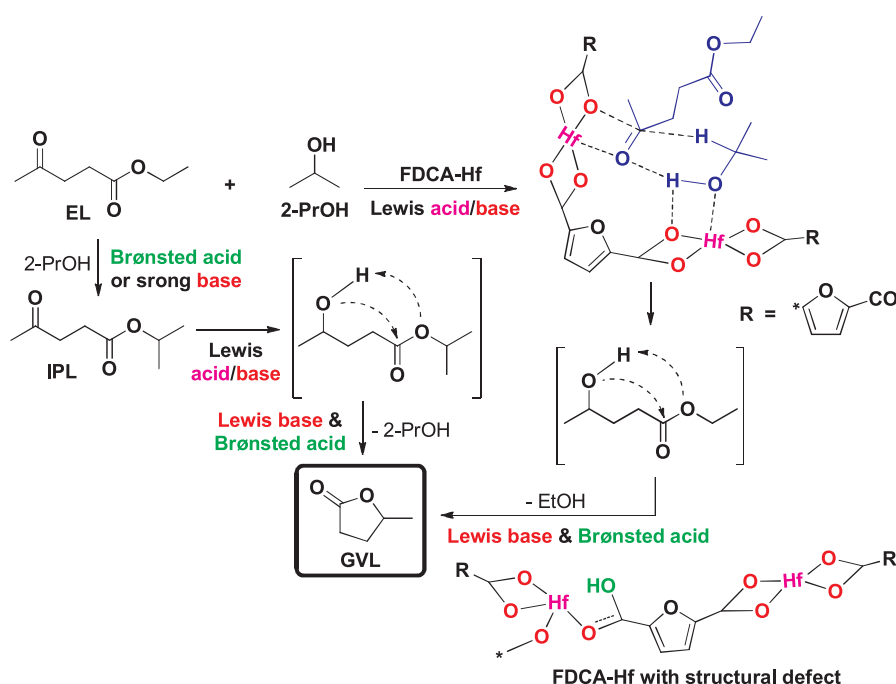


**Fig. 7.** Possible mechanism for producing GVL from EL catalyzed by FDCA-Hf.

sites were poisoned by excess pyridine (Py) and benzoic acid (Bz) illustrated by a previous report [40] to give FDCA-Hf-Py and FDCA-Hf-Bz, respectively. In comparison with FDCA-Hf, the treated counterparts all conformably exhibited inferior catalytic activity in the (trans)esterification of *Jatropha* oil under the optimal reaction conditions, giving biodiesel with yields in the order of FDCA-Hf (98%) > FDCA-Hf-Bz (83%) > FDCA-Hf-Na-300 (47%) > FDCA-Hf-Py (32%). These results demonstrated the synergistic effect of acid-base sites in the (trans)esterification, while the Brønsted acidic species might play a dominant role, which is in agreement with the proposed mechanism for the

catalytic lactonization of the in situ hydrogenated intermediate to GVL in Section 3.6.

#### 4. Conclusion

In summary, simple assembly of biomass-derived FDCA with Hf under template-free conditions gave a new porous and acid-base bi-functional FDCA-Hf hybrid. FDCA-Hf exhibited excellent activity (95–100% yields) and selectivity ( $\geq 97\%$ ) in the MPV reduction of diverse carbonyl compounds, especially for the conversion of EL to GVL,

**Table 3**  
MPV reduction of different biomass-derived carbonyl compounds to alcohols.

Entry	Substrate	Product	Temp (°C)	Time (h)	Conversion (%)	Selectivity (%)
1			90	1	100	> 99
2			90	1	100	> 99
3			100	1	> 99	99
4			100	1	99	98
5			100	2	100	> 99
6			100	3	100	> 99
7			100	5	98	97
8			100	5	97	99
9			100	4	95	> 99
10			100	4	96	> 99
11			120	6	99	99
12			120	4	98	97

Reaction conditions: 1 mmol substrate, 72 mg FDCA-Hf (16 mol% Hf), and 5 mL 2-PrOH.

and the (trans)esterification of acidic oils. Systematic studies indicated that the cooperative role of Lewis-acidic Hf, Lewis-basic carboxyl groups, and Brønsted acidic –OH species was the key factor responsible for the pronounced catalytic activity in cascade MPV reduction and lactonization. The FDCA-Hf hybrid had high thermal and chemical stability, and could be reused with constant performance in at least six consecutive cycles. The highly efficient and simply synthesized catalyst shows great potential for other acid-base cooperatively catalyzed reactions, and FDCA can be applied to prepare novel functional organic-inorganic hybrids.

## Acknowledgements

This work is financially supported by Nanjing Agricultural University (68Q-0603), International Postdoctoral Exchange Fellowship Program of China (20170026), Postdoctoral Science Foundation of China (2016M600422), and Jiangsu Postdoctoral Research Funding Plan(1601029A).

## Appendix A. Supplementary data

Supplementary data associated with this article can be found, in the online version, at <https://doi.org/10.1016/j.apcatb.2018.01.017>.

## References

- [1] P. Zhang, Y. Gong, H. Li, Z. Chen, Y. Wang, Solvent-free aerobic oxidation of hydrocarbons and alcohols with Pd@N-doped carbon from glucose, *Nat. Commun.* 4 (2013) 1593.
- [2] R.M. Vediappan Veeramani, S.M. Chen, B.S. Lou, J. Palanisamy, V.S. Vasanth, Biomass-derived functional porous carbons as novel electrode material for the practical detection of biomolecules in human serum and snail hemolymph, *Sci. Rep.* 5 (2015) 10141.
- [3] D. Kai, M.J. Tan, P.L. Chee, Y.K. Chua, Y.L. Yap, X.J. Loh, Towards lignin-based functional materials in a sustainable world, *Green Chem.* 18 (2016) 1175–1200.
- [4] H. Li, X. Liu, T. Yang, W. Zhao, S. Saravananurugan, S. Yang, Porous zirconium-furandicarboxylate microspheres for efficient redox conversion of biofuels, *ChemSusChem* 10 (2017) 1761–1770.
- [5] J. Guo, Y. Ping, H. Ejima, K. Alt, M. Meissner, J.J. Richardson, Y. Yan, K. Peter, D. von Elverfeldt, C.E. Hagemeyer, F. Caruso, Engineering multifunctional capsules through the assembly of metal-phenolic networks, *Angew. Chem. Int. Ed.* 53 (2014) 5546–5551.
- [6] J. Song, B. Zhou, H. Zhou, L. Wu, Q. Meng, Z. Liu, B. Han, Porous zirconium-phytic acid hybrid: a highly efficient catalyst for Meerwein-Ponndorf-Verley reductions, *Angew. Chem. Int. Ed.* 54 (2015) 9399–9403.
- [7] S. Narute, R. Parnes, F.D. Toste, D. Pappo, Enantioselective oxidative homocoupling and cross-coupling of 2-naphthols catalyzed by chiral iron phosphate complexes, *J. Am. Chem. Soc.* 138 (2016) 16553–16560.
- [8] F. Gelman, J. Blum, D. Avnir, Acids and bases in one pot while avoiding their mutual destruction, *Angew. Chem.* 113 (2001) 3759–3761.
- [9] K. Motokura, N. Fujita, K. Mori, T. Mizugaki, K. Ebitani, K. Kaneda, An acidic layered clay is combined with basic layered clay for one-pot sequential reactions, *J. Am. Chem. Soc.* 127 (2005) 9674–9675.
- [10] Y. Yang, X. Liu, X. Li, J. Zhao, S. Bai, J. Liu, Q. Yang, A yolk-shell nanoreactor with a basic core and an acidic shell for cascade reactions, *Angew. Chem. Int. Ed.* 51 (2012) 9164–9168.
- [11] H. Li, H. Wu, Q. Zhang, J. Liu, X. Liu, Y. Liu, S. Yang, Solid acid-base bifunctional catalysts in organic transformations, *Curr. Catal.* 2 (2013) 173–212.
- [12] E.L. Margelefsky, R.K. Zeidan, M.E. Davis, Cooperative catalysis by silica-supported organic functional groups, *Chem. Soc. Rev.* 37 (2008) 1118–1126.
- [13] E. Iglesias, D.G. Barton, J.A. Biscardi, M.J.L. Gines, S.L. Soled, Bifunctional pathways in catalysis by solid acids and bases, *Catal. Today* 38 (1997) 339–360.
- [14] M. Kanai, N. Kato, E. Ichikawa, M. Shibasaki, Recent progress in Lewis acid-Lewis base bifunctional asymmetric catalysis, *Pure Appl. Chem.* 77 (2005) 2047–2052.
- [15] M. Chia, J.A. Dumesic, Liquid-phase catalytic transfer hydrogenation and cyclization of levulinic acid and its esters to γ-valerolactone over metal oxide catalysts, *Chem. Commun.* 47 (2011) 12233–12235.
- [16] H.V. Lee, J.C. Juan, Y.H. Taufiq-Yap, Preparation and application of binary acid-base CaO-La<sub>2</sub>O<sub>3</sub> catalyst for biodiesel production, *Renew. Energy* 74 (2015) 124–132.
- [17] H. Li, Z. Fang, R.L. Smith, S. Yang, Efficient valorization of biomass to biofuels with bifunctional solid catalytic materials, *Prog. Energy Combust.* 55 (2016) 98–194.
- [18] Z. Zhang, K. Deng, Recent advances in the catalytic synthesis of 2,5-furandicarboxylic acid and its derivatives, *ACS Catal.* 5 (2015) 6529–6544.
- [19] N. Bouazza, M. Ouzzine, M.A. Lillo-Rodénas, D. Eder, A. Linares-Solano, TiO<sub>2</sub> nanotubes and CNT-TiO<sub>2</sub> hybrid materials for the photocatalytic oxidation of propene at low concentration, *Appl. Catal. B Environ.* 92 (2009) 377–383.
- [20] C. Maillet, P. Janvier, M. Pipelier, T. Praveen, Y. Andres, B. Bujoli, Hybrid materials for catalysis? Design of new phosphonate-based supported catalysts for the hydrogenation of ketones under hydrogen pressure, *Chem. Mater.* 13 (2001) 2879–2884.
- [21] H. Xu, J. Yan, Y. Xu, Y. Song, H. Li, J. Xia, C. Huang, H. Wan, Novel visible-light-driven AgX/graphite-like C<sub>3</sub>N<sub>4</sub> (X = Br, I) hybrid materials with synergistic photocatalytic activity, *Appl. Catal. B Environ.* 129 (2013) 182–193.
- [22] J. Di, J. Xi, Y. Ge, H. Li, H. Ji, H. Xu, Q. Zhang, H. Li, M. Li, Novel visible-light-driven CQDs/Bi<sub>2</sub>WO<sub>6</sub> hybrid materials with enhanced photocatalytic activity toward organic pollutants degradation and mechanism insight, *Appl. Catal. B Environ.* 168–169 (2015) 51–61.
- [23] H. Wu, Y.S. Chua, V. Krungleviciute, M. Tyagi, P. Chen, T. Yildirim, W. Zhou, Unusual and highly tunable missing-linker defects in zirconium metal-organic framework UiO-66 and their important effects on gas adsorption, *J. Am. Chem. Soc.* 135 (2013) 10525–10532.
- [24] F. Verpoort, T. Haemers, P. Roose, J.P. Maes, Characterization of a surface coating formed from carboxylic acid-based coolants, *Appl. Spectrosc.* 53 (1999) 1528–1534.
- [25] K.B. Lausund, O. Nilsen, All-gas-phase synthesis of UiO-66 through modulated atomic layer deposition, *Nat. Commun.* 7 (2016) 3578.
- [26] B. Tang, W. Dai, X. Sun, G. Wu, N. Guan, M. Hunger, L. Li, Mesoporous Zr-Beta zeolites prepared by a post-synthetic strategy as a robust Lewis acid catalyst for the ring-opening aminolysis of epoxides, *Green Chem.* 17 (2015) 1744–1755.
- [27] H. Li, Z. Fang, J. He, S. Yang, Orderly layered Zr-benzylphosphonate nanohybrids for efficient acid-base-mediated bifunctional/cascade catalysis, *ChemSusChem* 10 (2017) 681–686.
- [28] L. Bui, H. Luo, W.R. Gunther, Y. Roman-Leshkov, Domino reaction catalyzed by zeolites with Bronsted and Lewis acid sites for the production of γ-valerolactone from furfural, *Angew. Chem. Int. Ed.* 52 (2013) 8022–8025.
- [29] H.Y. Luo, D.F. Consoli, W.R. Gunther, Y. Román-Leshkov, Investigation of the reaction kinetics of isolated Lewis acid sites in Beta zeolites for the Meerwein-Ponndorf-Verley reduction of methyl levulinate to γ-valerolactone, *J. Catal.* 320 (2014) 198–207.
- [30] Y. Kuwahara, H. Kango, H. Yamashita, Catalytic transfer hydrogenation of biomass-derived levulinic acid and its esters to γ-valerolactone over sulfonic acid-functionalized UiO-66, *ACS Sustain. Chem. Eng.* 5 (2017) 1141–1152.
- [31] Q. Guo, F. Fan, E.A. Pidko, W.N.P. van der Graaff, Z. Feng, C. Li, E.J.M. Hensen, Highly active and recyclable Sn-MWW zeolite catalyst for sugar conversion to methyl lactate and lactic acid, *ChemSusChem* 6 (2013) 1352–1356.
- [32] J.Q. Bond, D.M. Alonso, D. Wang, R.M. West, J.A. Dumesic, Integrated catalytic conversion of γ-valerolactone to liquid alkenes for transportation fuels, *Science* 327 (2010) 1110–1114.
- [33] Z. Zhang, Synthesis of γ-valerolactone from carbohydrates and its applications, *ChemSusChem* 9 (2016) 156–171.
- [34] H. Li, Z. Fang, S. Yang, Direct conversion of sugars and ethyl levulinate into γ-valerolactone with superparamagnetic acid-base bifunctional ZrFeO<sub>x</sub> nanocatalysts, *ACS Sustain. Chem. Eng.* 4 (2016) 236–246.
- [35] H. Hu, P. Bhowmik, B. Zhao, M.A. Hamon, M.E. Itkis, R.C. Haddon, Determination of the acidic sites of purified single-walled carbon nanotubes by acid-base titration, *Chem. Phys. Lett.* 345 (2001) 25–28.
- [36] G. Cai, H.L. Jiang, A modulator-induced defect-formation strategy to hierarchically porous metal-organic frameworks with high stability, *Angew. Chem. Int. Ed.* 56 (2017) 563–567.
- [37] H. Reinsch, B. Bueken, F. Vermoortele, I. Stassen, A. Lieb, K.P. Lillerud, D. De Vos, Green synthesis of zirconium-MOFs, *CrystEngComm* 17 (2015) 4070–4074.
- [38] Z. Hu, I. Castano, S. Wang, Y. Wang, Y. Peng, Y. Qian, C. Chi, X. Wang, D. Zhao, Modulator effects on the water-based synthesis of Zr/Hf metal-organic frameworks: quantitative relationship studies between modulator, synthetic condition, and performance, *Cryst. Growth Des.* 16 (2016) 2295–2301.
- [39] H. Li, J. He, A. Riisager, S. Saravananurugan, B. Song, S. Yang, Acid-base bifunctional zirconium N-alkyltriphenylphosphonium hybrid for hydrogen transfer of biomass-derived carboxides, *Catal. Today* 26 (2016) 7722–7727.
- [40] X. Tang, H. Chen, L. Hu, W. Hao, Y. Sun, X. Zeng, L. Lin, S. Liu, Conversion of biomass to γ-valerolactone by catalytic transfer hydrogenation of ethyl levulinate over metal hydroxides, *Appl. Catal. B Environ.* 147 (2014) 827–834.
- [41] X. Tang, L. Hu, Y. Sun, G. Zhao, W. Hao, L. Lin, Conversion of biomass-derived ethyl levulinate into γ-valerolactone via hydrogen transfer from supercritical ethanol over a ZrO<sub>2</sub> catalyst, *RSC Adv.* 3 (2013) 10277–10284.
- [42] C. Xie, J. Song, B. Zhou, J. Hu, Z. Zhang, P. Zhang, Z. Jiang, B. Han, Porous hafnium phosphonate: novel heterogeneous catalyst for conversion of levulinic acid and esters into γ-valerolactone, *ACS Sustain. Chem. Eng.* 4 (2016) 6231–6236.
- [43] F. Li, L.J. France, Z. Cai, Y. Li, S. Liu, H. Lou, J. Long, X. Li, Catalytic transfer hydrogenation of butyl levulinate to γ-valerolactone over zirconium phosphates with adjustable Lewis and Brønsted acid sites, *Appl. Catal. B Environ.* 214 (2017) 67–77.
- [44] J. Song, L. Wu, B. Zhou, H. Zhou, H. Fan, Y. Yang, Q. Meng, B. Han, A new porous Zr-containing catalyst with a phenate group: an efficient catalyst for the catalytic transfer hydrogenation of ethyl levulinate to γ-valerolactone, *Green Chem.* 17 (2015) 1626–1632.
- [45] X. Tang, Z. Li, X. Zeng, Y. Jiang, S. Liu, T. Lei, Y. Sun, L. Lin, In situ catalytic hydrogenation of biomass-derived methyl levulinate to γ-valerolactone in methanol, *ChemSusChem* 8 (2015) 1601–1607.
- [46] K. Yan, T. Lafleur, J. Liao, Facile synthesis of palladium nanoparticles supported on multi-walled carbon nanotube for efficient hydrogenation of biomass-derived levulinic acid, *J. Nanopart. Res.* 15 (2013) 1906.
- [47] K. Yan, T. Lafleur, C. Jarvis, G. Wu, Clean and selective production of γ-valerolactone from biomass-derived levulinic acid catalyzed by recyclable Pd

- nano particle catalyst, *J. Clean. Prod.* 72 (2014) 230–232.
- [48] S.G. Wettstein, J.Q. Bond, D.M. Alonso, H.N. Pham, A.K. Datye, J.A. Dumesic, RuSn bimetallic catalysts for selective hydrogenation of levulinic acid to  $\gamma$ -valerolactone, *Appl. Catal. B Environ.* 117–118 (2012) 321–329.
- [49] X.L. Du, Q.Y. Bi, Y.M. Liu, Y. Cao, K.N. Fan, Conversion of biomass-derived levulinate and formate esters into  $\gamma$ -valerolactone over supported gold catalysts, *ChemSusChem* 4 (2011) 1838–1843.
- [50] L. Deng, J. Li, D.M. Lai, Y. Fu, Q.X. Guo, Catalytic conversion of biomass-derived carbohydrates into  $\gamma$ -valerolactone without using an external H<sub>2</sub> supply, *Angew. Chem. Int. Ed.* 48 (2009) 6529–6532.
- [51] N.A.S. Ramli, N.A.S. Amin, Fe/HY zeolite as an effective catalyst for levulinic acid production from glucose: characterization and catalytic performance, *Appl. Catal. B Environ.* 163 (2015) 487–498.
- [52] L. Jiang, L. Zhou, J. Chao, H. Zhao, T. Lu, Y. Su, X. Yang, J. Xu, Direct catalytic conversion of carbohydrates to methyl levulinate: synergy of solid Brønsted acid and Lewis acid, *Appl. Catal. B Environ.* 220 (2018) 589–596.
- [53] K. Yan, Y. Yang, J. Chai, Y. Lu, Catalytic reactions of gamma-valerolactone: a platform to fuels and value-added chemicals, *Appl. Catal. B Environ.* 179 (2015) 292–304.
- [54] M. Sudhakar, V. VijayKumar, G. Naresh, M. Lakshmi Kantam, S.K. Bhargava, A. Venugopal, Vapor phase hydrogenation of aqueous levulinic acid over hydroxyapatite supported metal (M = Pd, Pt, Ru, Cu, Ni) catalysts, *Appl. Catal. B Environ.* 180 (2016) 113–120.
- [55] S. Song, L. Di, G. Wu, W. Dai, N. Guan, L. Li, Meso-Zr-Al-beta zeolite as a robust catalyst for cascade reactions in biomass valorization, *Appl. Catal. B Environ.* 205 (2017) 393–403.
- [56] C. García-Sancho, I. Fúnez-Núñez, R. Moreno-Tost, J. Santamaría-González, E. Pérez-Inestrosa, J.L.G. Fierro, P. Maireles-Torres, Beneficial effects of calcium chloride on glucose dehydration to 5-hydroxymethylfurfural in the presence of alumina as catalyst, *Appl. Catal. B Environ.* 206 (2017) 617–625.
- [57] S. Song, S. Yao, J. Cao, L. Di, G. Wu, N. Guan, L. Li, Heterostructured Ni/NiO composite as a robust catalyst for the hydrogenation of levulinic acid to  $\gamma$ -valerolactone, *Appl. Catal. B Environ.* 217 (2017) 115–124.
- [58] H. Li, Z. Fang, S. Yang, Direct catalytic transformation of biomass derivatives into biofuel component  $\gamma$ -valerolactone with magnetic nickel-zirconium nanoparticles, *ChemPlusChem* 81 (2016) 135–142.
- [59] M.M. Antunes, S. Lima, P. Neves, A.L. Magalhães, E. Fazio, F. Neri, M.T. Pereira, A.F. Silva, C.M. Silva, S.M. Rocha, M. Pillinger, A. Urakawa, A.A. Valente, Integrated reduction and acid-catalysed conversion of furfural in alcohol medium using Zr,Al-containing ordered micro/mesoporous silicates, *Appl. Catal. B Environ.* 182 (2016) 485–503.